Int. J. Heat Mass Transfer. Vol. 31, No. 2, pp. 301–309, 1988
Printed in Great Britain

0017–9310/88 $3.00 + 0.00

Effects of thermal dispersion on forced convection in fibrous media

M. L. HUNT and C. L. TIEN
Department of Mechanical Engineering, University of California, Berkeley, CA 94720, U.S.A.

(*Received* 31 *August* 1987)

Abstract—This experimental study investigates non-Darcian flow and heat transfer in high-porosity fibrous media. It considers forced convection through materials of different permeability, porosity and thermal conductivity. The results show that the porous medium enhances heat transfer from a surface as compared to predicted results for slug or for laminar flow in a channel. This enhancement results from dispersion, a non-Darcian phenomenon describing the intra-pore mixing that develops as the fluid moves past the solid particles. The dispersive transport increases with flow rate and permeability, and at large Reynolds numbers overwhelms transport from solid conduction within the fibrous medium. To predict dispersion, this work develops a simple model based on the flow conditions and types of porous media. Results from the experiment and model demonstrate the effects of dispersion and the adequacy of the homogeneous fluid–solid energy equation to model the transport.

INTRODUCTION

THIS PAPER experimentally and analytically examines flow and heat transfer in constant-porosity fibrous media. The focus of this work is on high Reynolds number forced flows when non-Darcian effects such as thermal dispersion and inertial drag are predominant. These effects become important when modeling forced convection in compact heat exchangers or regenerators. The analysis is also important in modeling natural convection in fibrous insulation, since it experimentally demonstrates the magnitude of thermal dispersion and presents an analytical model of the phenomenon.

Traditional porous-media analyses utilize Darcian or slug flow models and neglect the non-Darcian effects such as the viscous shear force along the solid boundaries, the inertial convective force and thermal dispersion [1–4]. When a porous medium lies adjacent to an impermeable surface the velocity profile must satisfy the no-slip condition. Throughout the porous medium the fluid moves in tortuous paths and recirculates at the back of the solid fibers. This convective or inertial effect increases with Reynolds number, yielding an increase in pressure drop across the medium. If a temperature or concentration gradient occurs across the fibers, the recirculation or dispersion mixes the fluid and increases the net transport.

This study and other previous works incorporate these effects through a volume-averaging process [5, 6]. The momentum equation is determined by volume averaging the Navier–Stokes equations and relating the drag force from the presence of the solid phase to the Darcian force. The energy equation results from separately averaging the fluid and solid phases and combining the equations with an effective conductivity by assuming a small variation in the temperature gradient [4, 5]. The averaging method, however, eliminates microscopic phenomena such as local recirculation or dispersion, and thus the equations rely on additional empirical relations for closure. A recent analytical mass transfer study by Koch and Brady [7] uses ensemble averaging to develop relations for molecular dispersion in fibrous media. Their analysis focuses on unconfined media, and therefore does not include effects of global variations in velocity or concentration. The results do demonstrate a functional relationship between the dispersion conductivity and the Reynolds number for mass transfer in fibrous media. Two studies examine momentum, heat and mass transfer in a semi-infinite fibrous medium [1, 2]. These works include the viscous shear force and the inertial effect, but the thermal and mass transfer analyses do not include dispersion. The mass transfer experiment, however, is for high Schmidt numbers, which for the experimental conditions obscures any dispersion effect [4].

The experimental investigation involves a two-dimensional boundary layer flow along a constant temperature surface at the entrance of a channel. The focus is to analytically and experimentally quantify dispersion and to predict the heat transfer from the heated surface. The experiment uses materials of different conductivities, porosities and permeabilities to provide a range of flow and thermal conditions. The analysis is based on volume averaging and employs a homogeneous or single energy-equation model. Dispersion is included by relating the dispersive flux to the macroscopic temperature gradient and an empirical dispersion conductivity. The experimental results indicate that the dispersion conductivity can be equated to a product of the local velocity, square root

NOMENCLATURE

A	dispersion coefficient
c_P	specific heat at constant pressure
D	molecular diffusivity
Da_x	square root of the inverse Darcy number, $x/\sqrt{K}$
f	inertial coefficient
$\bar{h}$	length-averaged heat transfer coefficient
K	permeability
k	thermal conductivity
L	channel length
Nu_x	local Nusselt number
$\overline{Nu}$	length-averaged Nusselt number
P	pressure
Pe_m	mass diffussion Peclet number, $u_a\sqrt{K}/D_f$
Pr	Prandtl number, $\mu/\rho\alpha_o$
Re_D	Darcian Reynolds number, $\rho u_D\sqrt{K}/\mu$
Re_a	average Reynolds number, $\rho u_a\sqrt{K}/\mu$
T	temperature
t	channel height
U	dimensionless velocity, u/u_D
u	stream-wise velocity
u_D	Darcian velocity, $-(K/\mu)(dP/dx)$
w	channel width
X	dimensionless length, $x\varepsilon/(\sqrt{k}\,Re_D\,Pr)$
x	stream-wise direction
Y	dimensionless length, $y(\varepsilon/K)^{1/2}$
y	cross-stream direction.

Greek symbols

α	thermal diffusivity, $k/\rho c_P$
γ	dispersion coefficient
ε	porosity
Θ	dimensionless temperature
μ	dynamic viscosity
ρ	density.

Subscripts and superscripts

a	average
b	bulk
c	centerline
D	Darcian
d	dispersion
f	fluid
i	inlet
o	stagnant
s	solid
w	wall
∞	infinity
$\overline{\ }$	length averaged
$\sim$	spatially varying.

of the permeability and a constant. The experiment also demonstrates that dispersion is significantly larger than molecular, solid conduction for high Reynolds number flows. However, a homogeneous energy equation suffices to model the flow.

ANALYTICAL FORMULATION

Transport in porous media involves complex flow patterns around solid particles or fibers. Due to the random orientations of the solid phase, exact solutions to the detailed local flow field are impossible. Instead tenable solutions are found by volume averaging the governing equations. This averaging, however, obscures local pore phenomena that contribute to the global transport, and hence requires the use of empirical relations for closure. The averaging is performed over a volume smaller than the overall dimensions but which contains a representative number of pores or fibers. For a channel or two-dimensional boundary layer the averaging volume is represented by a cylindrical tube aligned perpendicular to the flow direction such as depicted in Fig. 1.

The steady volume-averaged continuity and momentum equations for forced convection in a porous medium are [1, 3, 4]

$$\nabla\cdot\langle\underline{u}\rangle = 0 \tag{1}$$

$$\frac{\rho}{\varepsilon^2}\langle\underline{u}\cdot\nabla\underline{u}\rangle = -\nabla\langle P\rangle - \frac{\mu}{K}\langle\underline{u}\rangle - \rho\frac{f}{\sqrt{K}}|\langle\underline{u}\rangle|\langle\underline{u}\rangle + \frac{\mu}{\varepsilon}\nabla^2\langle\underline{u}\rangle \tag{2}$$

where $\langle\ \rangle$ represents a volume-averaged quantity, $\underline{u}$ and P are the local velocity and pressure, ρ and μ the fluid density and viscosity, ε the porosity, f the inertial coefficient and K the permeability. The permeability and inertial coefficient are determined from empirical relations and depend on the fiber size and porosity of the medium [8]. Unlike packed-sphere beds, the porosity and permeability for fibrous media are constant even close to the solid boundary.

The momentum equation contains terms similar to those found in the Navier–Stokes equations, along with the flow resistance terms inherent to porous-media studies. The first two terms on the right-hand side represent the pressure drop and the Darcian resistance, respectively. The Darcian term represents the form drag caused by the presence of the porous medium. If these two terms are isolated from the others, the equation reduces to Darcy's law, a uniform-velocity approximation for flow in porous media. For higher Reynolds number flows, the Darcian relation is corrected by adding the third term. This term accounts for the larger pressure drop caused by the local acceleration and separation around the

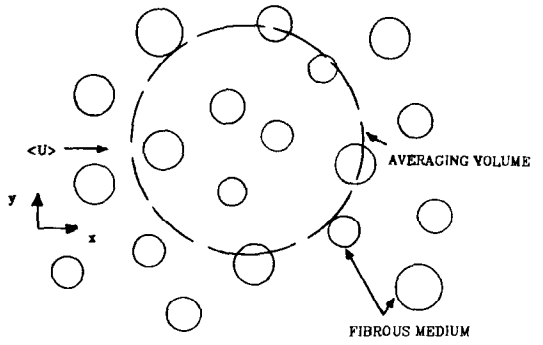

FIG. 1. Diagram of coordinate system and averaging volume.

solid particles. The fourth term on the right-hand side of the equation is an additional pressure loss caused by viscous shear along the solid boundary. By including this term, the no-slip boundary condition is satisfied. The left-hand side of the equation is the volume-averaged convective term and is usually neglected except when a velocity gradient exists in the flow direction such as in the developing region of the flow [1].

The volume-averaged homogeneous energy equation is [1, 3, 4]

$$\rho c_P \langle \underline{u} \rangle \cdot \nabla \langle T \rangle = \nabla \cdot (k_o \nabla \langle T \rangle) - \rho c_P \nabla \cdot \langle \tilde{u} \tilde{T} \rangle \quad (3)$$

where ρ and c_P are the fluid density and heat capacity, and k_o is the effective stagnant conductivity. The stagnant conductivity, k_o, depends on the porosity and conductivities of the fluid and solid, thus accounting for the molecular conduction within both phases. Its bulk value is determined from an empirical model [9]. The use of a homogeneous equation assumes locally equivalent temperature gradients between the fluid and solid phases [4, 5].

The convective term is decomposed into the average and spatially varying components. The additional flux arises from mixing as the fluid separates and recombines around the fibers. If a temperature gradient exists in the system the process yields a net transport. Therefore dispersion can be viewed as a diffusive process related to the overall temperature gradient and a dispersion conductivity

$$\rho c_P \langle \tilde{u} \tilde{T} \rangle = -k_d \nabla \langle T \rangle. \quad (4)$$

Experimental measurements for packed beds relate the dispersion conductivity to a product of the average velocity, particle diameter and a constant equal to 0.1 [3]. A similar approach is used by Koch and Brady [7] to model dispersion in fibrous media. Their analysis uses ensemble averaging and defines the dispersion conductivity as the product of the velocity, fiber thickness and a constant dependent on the porosity. Using this approach, the dispersion conductivity equals

$$k_d = \rho c_P \gamma \sqrt{K} u \quad (5)$$

where γ is the dispersion coefficient and the square root of the permeability relates to the fiber thickness.

For a two-dimensional flow in constant-porosity media, the governing equations are

$$0 = -\frac{d\langle P \rangle}{dx} - \frac{\mu}{K}\langle u \rangle - \rho \frac{f}{\sqrt{K}}\langle u \rangle^2 + \frac{\mu}{\varepsilon}\frac{d^2\langle u \rangle}{dy^2} \quad (6)$$

$$\langle u \rangle \frac{\partial \langle T \rangle}{\partial x} = \alpha_o \frac{\partial}{\partial y}\left[\left(1 + \frac{k_d}{k_o}\right)\frac{\partial \langle T \rangle}{\partial y}\right]. \quad (7)$$

The momentum equation neglects the convective term since the velocity is fully developed and varies only in the cross-stream direction due to the presence of the solid surface. Because of the large Reynolds numbers, the energy equation omits the diffusive flux in the stream-wise direction. These equations can be written in non-dimensional form as

$$0 = 1 - U - f\, Re_D\, U^2 + \frac{d^2U}{dY^2} \quad (8)$$

$$U \frac{\partial \Theta}{\partial X} = \frac{\partial}{\partial Y}\left[(1 + \gamma\, Re_D\, Pr\, U)\frac{\partial \Theta}{\partial Y}\right] \quad (9)$$

using the following definitions:

$$u_D = -\frac{K}{\mu}\frac{d\langle P \rangle}{dx}, \quad U = \frac{\langle u \rangle}{u_D}, \quad Re_D = \frac{\rho u_D \sqrt{K}}{\mu},$$

$$Y = y\left(\frac{\varepsilon}{K}\right)^{1/2}, \quad X = x\frac{\varepsilon}{\sqrt{K}\, Re_D\, Pr},$$

$$\Theta = \frac{\langle T \rangle - \langle T_i \rangle}{\langle T_w \rangle - \langle T_i \rangle}. \quad (10)$$

If the boundary term is neglected in the momentum equation, then the equation reduces to the modified Darcy relation with the velocity equal to

$$U_a = [-1 + (1 + 4f\, Re_D)^{1/2}]/(2f\, Re_D). \quad (11)$$

A form of this equation determines the permeability and inertial coefficient as shown in the experimental section. The velocity, U_a, represents the average velocity in a channel, and for a semi-infinite flow equals the free-stream velocity. Using this velocity the average Reynolds number is, $Re_a = Re_D\, U_a$, a more physical parameter than the Darcian Reynolds number, Re_D, since it represents the actual flow velocity and not the pressure drop.

Using the slug-flow approximation given by equation (11) with the boundary conditions for a semi-infinite medium

$$\Theta = 0 \text{ at } X = 0 \text{ and } Y \to \infty, \quad \Theta = 1 \text{ at } Y = 0 \quad (12)$$

and integrating the energy equation yields

$$\Theta = 1 - \mathrm{erf}\{Y/2[(1 + \gamma\, Re_a\, Pr)X/U_a]^{-1/2}\} \quad (13)$$

where erf is the error function. The length-averaged Nusselt number is then

$$\overline{Nu} = \frac{\bar{h}L}{k_o} = \frac{1}{L}\int_0^L Nu_x\, dx$$

$$= 2\left[\frac{1}{\pi}Re_a\, Pr\, Da_L(1 + \gamma\, Re_a\, Pr)\right]^{1/2} \quad (14)$$

where Da_L is the inverse Darcy number, $Da_L = L/\sqrt{K}$. If $\gamma = 0$, the heat transfer coefficient increases with the

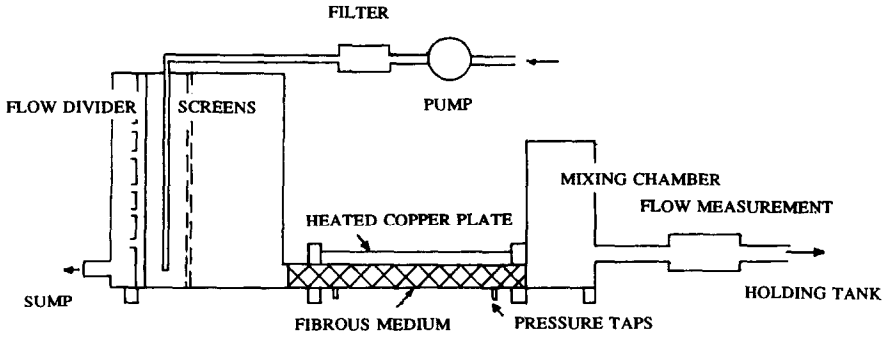

FIG. 2. Schematic of experimental apparatus.

square root of the downstream distance and average velocity.

The full momentum equation, equation (8), is identical to the first integration of the third-order differential equation governing flow in a wedge-shaped region [10]. The equation is solved by multiplying by dU/dY and integrating using the boundary conditions $dU/dY = 0$ as $U \to U_a$. The equation after rearranging terms is

$$Y = \int_0^U (dU^*/[2(U_a - U^*) + (U^{*2} - U_a^2) + \tfrac{2}{3} f\, Re_D (U^{*3} - U_a^3)]^{1/2}). \quad (15)$$

This equation is an elliptic integral and is easily integrated numerically.

EXPERIMENTAL APPARATUS AND PROCEDURE

Because the internal structure of a fibrous medium is complex, local measurements within the medium are difficult to perform. The experiment, depicted in Fig. 2, is used to determine the average heat transfer rate from a heated surface adjacent to a porous matrix. The constant-porosity medium was placed in the channel of length, $L = 15.24$ cm, width, $w = 5.08$ cm, and height, $t = 1.27$ cm. Flush with the porous surface is a thick (1.27 cm) copper plate that acted as a constant temperature surface containing ten copper–constantan thermocouples. On this plate are four strip heaters connected to separate variable power supplies. The opposite wall is made of thick plexiglas and contains four thermocouples to check the adiabatic wall temperature. Throughout the cases examined, the thermal boundary layer was so thin that the adiabatic wall remained at the inlet fluid temperature.

The working fluid was water that had been heated and allowed to cool to room conditions to remove any dissolved air. The water was held in a large auxiliary tank and drawn via a variable speed pump from this tank through a filter into the upstream reservoir. This reservoir has a series of adjustable overflow dividers to provide a constant pressure head. Reservoir screens dampen fluctuations in the flow before entering the channel. An additional section of porous media was placed in the upstream channel region to provide a region for hydraulic development.

The water flowed through the channel into another smaller downstream reservoir. This reservoir has adjustable slats to mix the fluid and to ensure an accurate exit bulk temperature. To determine the flow rate, the fluid was collected after exiting the channel over a specific time interval. Along the bottom of the channel are two pressure taps that connect to a U-tube manometer for pressure drop measurements.

The experiment was performed using seven different pieces of high-porosity foam material. Each piece consists of continuously connected fibers formed in a rigid open-cell matrix. The materials are isotropic, uniform in pore spacing and cut so that the sides were flush with the channel walls. There are three different solid-phase materials: aluminum ($k_s = 180$ W m^{-1} °C^{-1}), nickel ($k_s = 70$ W m^{-1} °C^{-1}), and carbon ($k_s = 6$ W m^{-1} °C^{-1}). The materials offer a range of porosity, permeability and effective conductivity.

Before beginning the experiments the channel was used without a porous medium to evaluate the procedure and external heat losses. The results compared with known solutions for thermally-developing laminar channel flow with one constant temperature and one adiabatic wall [11]. With the porous medium the experimental procedure was conducted in two parts. First under adiabatic conditions the pressure drop was measured for a range of flow rates. From this adiabatic data the permeability and inertial coefficients for the porous medium were calculated using a rearranged version of the modified Darcy equation

$$-\frac{dP}{dx}\frac{1}{\mu u_a} = \frac{1}{K} + \rho \frac{f}{\sqrt{K}}\frac{u_a}{\mu}. \quad (16)$$

By plotting the quantity $(-1/\mu u_a)(dP/dx)$ as a function $\rho u_a/\mu$ for a range of flow rates, the permeability is defined as the intercept and the inertial coefficient is determined from the slope [8].

After obtaining the permeability and inertial coefficient of the material, the heat transfer experiments were performed to obtain the length-averaged heat transfer coefficients. The inlet, outlet and plate

Table 1. Parameters for fibrous materials

Piece	1	2	3	4	5	6	7
Material	C	C	Ni	Al	Al	Al	Al
Porosity, ε	0.97	0.97	0.97	0.97	0.97	0.94	0.94
Pore density, ϕ [pore cm^{-1}]	5	10	10	10	5	10	4
Permeability, $K \times 10^7$ [m^2]	4.1	0.92	0.96	0.80	4.8	0.53	17.0
Inertial coefficient, f	0.11	0.077	0.089	0.050	0.17	0.10	0.30
Conductivity ratio, k_o/k_f	1.05	1.05	1.22	1.37	1.37	1.61	1.61

temperatures were measured along with the input power to verify the net heat transfer calculation. The flow rate and pressure drop were re-evaluated using the adiabatic permeability and inertial coefficient. This allowed the velocity measurement to be rechecked and ensured that the system had not deviated from air bubbles trapped within the porous medium.

Using the thermal results, the length-averaged heat transfer coefficient is

$$\bar{h} = q/(T_w - T_i) = \rho c_P (T_o - T_i) u_a t/[L(T_w - T_i)] \quad (17)$$

with the length-averaged Nusselt number, $\overline{Nu} = \bar{h}L/k_o$. For channel flows the heat transfer coefficient can also be defined using the bulk temperature

$$\bar{h}_b = q/(T_w - T_b) = \rho c_P (T_o - T_i) u_a t/[L(T_w - T_b)] \quad (18)$$

with the bulk-temperature Nusselt number, $\overline{Nu}_B = \bar{h}_b L/k_o$.

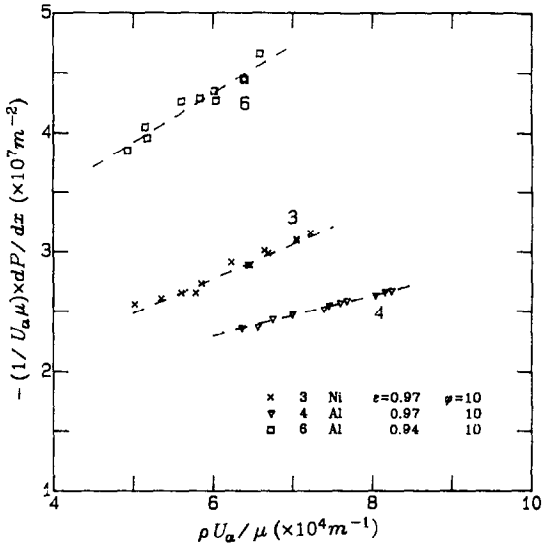

FIG. 3. Graphical determination of permeability and inertial coefficient.

RESULTS AND DISCUSSION

The experimental investigation uses seven different pieces of porous media. Table 1 lists these pieces and the corresponding flow and thermal parameters. Figure 3 shows for three pieces of porous media the experimental data used to determine the permeability and inertial coefficient as suggested by equation (15). The flow parameters from the other materials are determined in a similar manner. As Table 1 demonstrates, the open matrices of lower pore density result in higher permeabilities, and thicker fiber matrices of lower porosity produce larger inertial coefficients. The table also lists the effective conductivity of the different pieces. This is determined from the statistical model of ref. [9] and reflects the solid and liquid conductivity, porosity and fiber type.

The velocity profile is determined using two different methods, numerically integrating the second-order differential equation, equation (8), and by evaluating the elliptic integral, equation (15). For channel flows the centerline velocity replaces the average velocity, U_a, in equation (15) and in the boundary conditions for equation (8), $U = 0$ at $Y = 0$, and $U = U_c$ at the channel midplane. However, the centerline velocity is not explicitly known and therefore the process is iterated until the total flow rate is correct. The differential equation, equation (8), is easier to use, but the elliptic integral, equation (15), is valuable in checking the numerical scheme.

Figure 4 demonstrates the effect of different porous materials on the velocity field for flow in the channel. The average velocity is the same for each profile. Without the porous medium the flow is parabolic; with the porous medium the velocity is uniform in the main stream with a steep gradient near the wall. For the higher-permeability material, $K = 5 \times 10^{-6}$ m^2, $f = 0.3$, $Re_a = 80$, the momentum boundary layer is slightly thicker and the main stream velocity is higher than for the lower-permeability material, $K = 5 \times 10^{-8}$ m^2, $f = 0.08$, $Re_a = 8$. For each of these flows the centerline velocity is approximately 1% greater than the average velocity. As shown by ref. [1], the momentum boundary layer only grows in the entrance region of the flow. For this experiment the entrance region is neglected by placing a piece of fiber material upstream of the heated plate. Hence the momentum boundary layer thickness is constant throughout the channel.

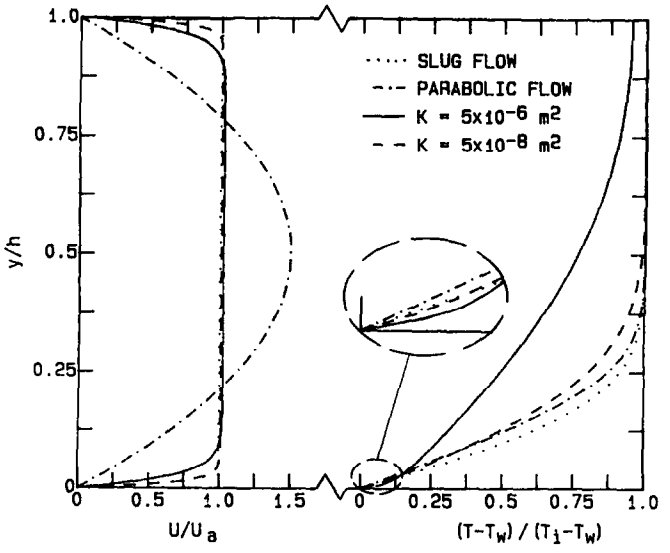

FIG. 4. Velocity and temperature profiles for slug and laminar flow, and for flow through fibrous media in a channel.

The energy equation, equation (9), is integrated using a finite-different technique. The numerical formulation uses a marching scheme based on upwind differences in the flow direction and an implicit central-difference scheme for the cross-stream direction. The numerical model is verified by calculating the semi-infinite slug flow solution and comparing the results to the solution given in equation (13) for $\gamma = 0$. The solutions are also checked by varying the grid spacing.

Figure 4 also depicts the corresponding temperature profiles at the channel exit for flow confined between an adiabatic and a constant temperature surface. The ratio of effective to fluid conductivity is unity and the value of the dispersion coefficient is 0.025 as determined from the experiment and discussed in the following paragraphs. For the porous-medium profiles the temperature gradients at the wall are sharper than the parabolic or slug flow profiles. The effect of the heated wall has penetrated further into the channel containing the fibrous medium. Hence dispersion, like turbulent transport, increases the net flux from the boundary while mixing the fluid in the main stream, yielding a sharper temperature profile.

Figure 5 shows the variation of the local bulk-temperature Nusselt number for these four flows with the same average velocity. The results for the high-permeability material show a higher heat transfer rate due to dispersion. The entrance lengths appear to be similar since the flow rate and channel size are the same.

The experimental heat transfer results from the different types of porous media are shown in Fig. 6. Because of the number of parameters involved, the results can be presented as a function of many different non-dimensional groups. To first examine the influence of the porous medium solely as a function of the

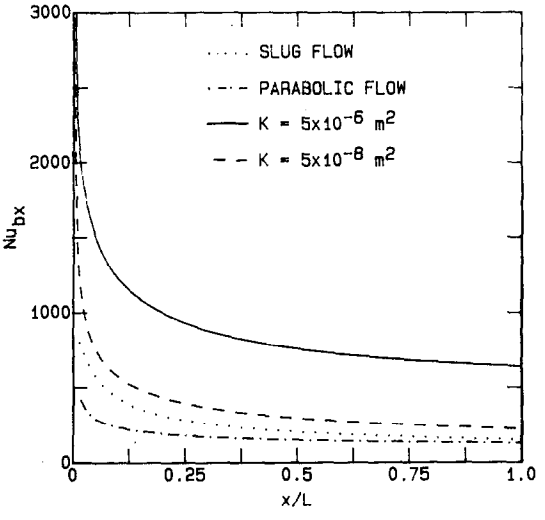

FIG. 5. Local bulk-temperature Nusselt numbers for slug and laminar flow, and for flow through fibrous media in a channel.

flow rate, independent of the permeability or solid conductivity, the data are presented as a function of the Reynolds–modified-Darcy parameter, $Re_a Da_L = \rho u_a L/\mu$, and the bulk-temperature Nusselt number based on fluid conductivity, $\overline{Nu}_{bf} = \bar{h}_b L/k_f$. Also shown in the figure are the theoretical predictions for the Nusselt numbers for slug and laminar flow in a channel [11]. As the figure demonstrates, the porous material significantly enhances the heat transfer. For any of the materials the difference between the experimental results and the slug-flow predictions increases with permeability and flow rate suggesting the dependence of dispersion on both of these quantities as assumed in equation (5). The highest Nusselt numbers correspond to the material of the highest permeability,

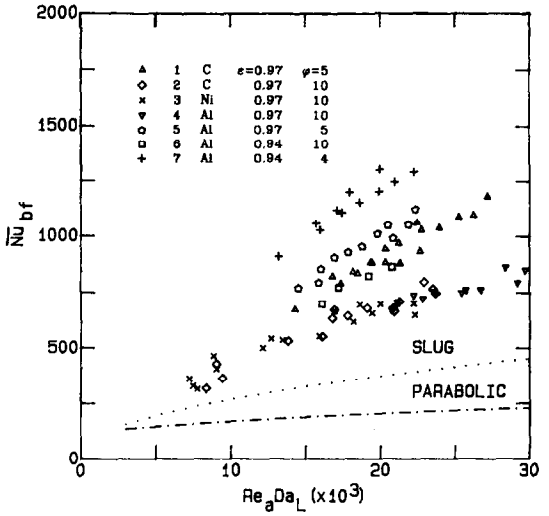

FIG. 6. Bulk-temperature Nusselt numbers as a function of Reynolds number based on channel length for different porous materials and flows.

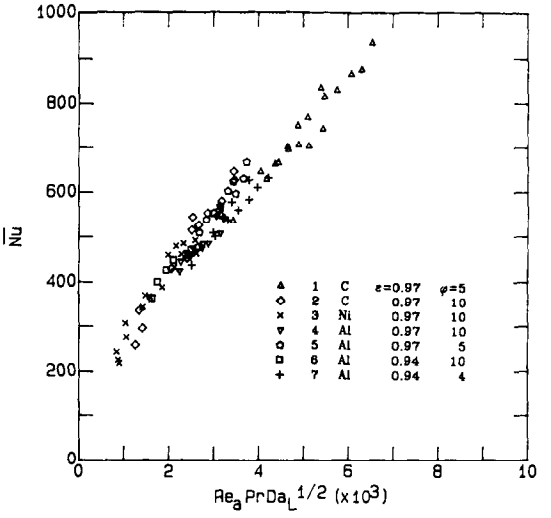

FIG. 8. Average Nusselt numbers as a function of Reynolds–Prandtl–modified-Darcy number.

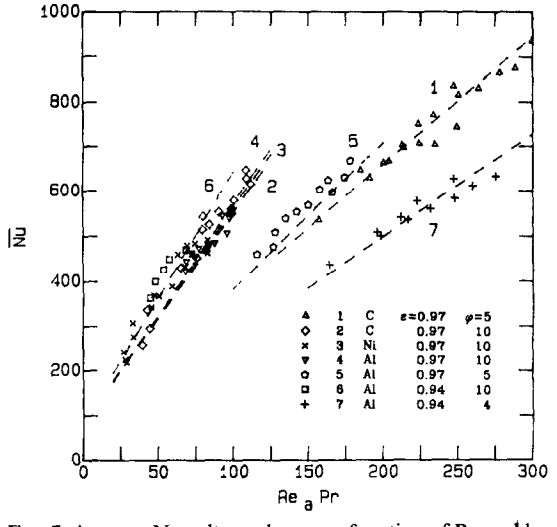

FIG. 7. Average Nusselt numbers as a function of Reynolds–Prandtl number based on permeability.

Piece 7. Pieces 2–4 have similar flow parameters and though the materials are of different conductivities, the heat transfer results are similar. For this high porosity, the fibers are thin and conduction may not be significant; instead dispersion dominates any molecular conduction, resulting in heat transfer seemingly independent of solid conductivity. However, for lower-porosity materials, such as Piece 6, the heat transfer has increased compared to that for Pieces 2–4 since the material is slightly more conductive.

In Fig. 7 the heat transfer data are presented as a function of the Reynolds–Prandtl number based on permeability, $Re_a Pr = \rho u_a \sqrt{K}/\mu$, and the Nusselt number based on effective conductivity, $\overline{Nu} = \bar{h}L/k_o$. The data fall in distinct groups depending on the permeability of the material. The dashed lines are numerical calculations for the hydrodynamically developed, thermal entrance region in a channel with one constant temperature and one adiabatic surface. The calculations for each piece of fibrous media are based on the effective conductivity and the experimentally measured permeability and inertial coefficient listed in Table 1. With a dispersion coefficient of 0.025, the calculated lines fall close to the experimental data indicating the simple model for dispersion, equation (5), is suitable for the flow conditions considered.

If the data in Fig. 7 are reduced using the grouping, $Re_a Pr\, Da_L^{1/2}$, the data collapse to a single line in Fig. 8. This grouping is also suggested by the modified-Darcian results, equation (14), for $Re_a Pr$ greater than one. Thus for high Reynolds number flows the Nusselt number is directly proportional to the average flow rate and a characteristic length, $(L\sqrt{K})^{1/2}$

$$\overline{Nu} \propto Re_a Pr\, Da_L^{1/2} = u_a L^{1/2} K^{1/4}/\alpha_o. \qquad (19)$$

This relation also suggests the heat transfer coefficient is independent of conductivity for higher Reynolds number flow as indicated by the experimental data. Furthermore, the results demonstrate the adequacy of the homogeneous energy equation to model the transport for the flow conditions considered.

The theoretical lines are based on a dispersion coefficient, γ, equal to 0.025 and the empirical dispersion conductivity given in equation (5). The analysis by Koch and Brady [7] develops a similar relation showing dispersion directly proportional to the local velocity at higher Reynolds numbers. Their work suggests the following relation:

$$\frac{D_d}{D_f} = \frac{3}{320}\pi^3 \left|\ln\frac{1}{1-\varepsilon}\right|^{-1} Pe_m = A\, Pe_m \qquad (20)$$

where D is the molecular diffusivity, Pe_m the mass

diffusion Peclet number, $Pe_m = u_a\sqrt{K}/D_f$, and A is a constant similar to γ but dependent on porosity. For a porosity of 0.97 the coefficient A is 0.083, approximately three times larger than the experimental value, γ. However, the semi-theoretical relation given for the permeability appears to underestimate the measured value. For Pieces 2–4 the average fiber radius is 0.2 mm and the permeability is about 1×10^{-7} m^2. Using this value in Koch and Brady's permeability relationship, the experimental permeability would correspond to a radius of about 0.075 mm, about half the actual size. However, the product of the dispersion coefficient and the square root of permeability are close suggesting the ratio of dispersion to molecular diffusivity (or conductivity) are similar for the present heat transfer experiment and the theoretical analysis of Koch and Brady [7].

CONCLUSIONS

The present experiment and analysis demonstrate the increase in heat transfer from thermal dispersion. The model develops a relation for dispersion by equating the dispersion conductivity to a product of the velocity, square root of the permeability and an experimental constant determined from seven different pieces of fibrous media. Though the focus of the work is forced convection, the same dispersion model can be applied to natural convection problems such as transport in thermal insulation. By using materials of different conductivities, experiments demonstrate that dispersion overwhelms transport from solid conduction. However, a single homogeneous energy equation suffices to model the transport.

REFERENCES

1. K. Vafai and C. L. Tien, Boundary and inertia effects on flow and heat transfer in porous media, *Int. J. Heat Mass Transfer* **24,** 195–203 (1981).
2. K. Vafai and C. L. Tien, Boundary and inertia effects on convective mass transfer in porous media, *Int. J. Heat Mass Transfer* **25,** 1183–1190 (1982).
3. M. L. Hunt and C. L. Tien, Non-Darcian convection in cylindrical packed beds, *Proceedings of the Second ASME/JSME Thermal Engineering Joint Conference*, Vol. 21, pp. 433–438 (1987).
4. C. L. Tien and M. L. Hunt, Boundary-layer flow and heat transfer in porous beds, *Chem. Engng Process.* **21,** 53–63 (1987).
5. R. G. Carbonell and S. Whitaker, Heat and mass transfer in porous media. In *Fundamentals of Transport Phenomena in Porous Media* (Edited by J. Bear and M. Y. Corapcioglu), NATO ASI Series, pp. 123–198 (1984).
6. J. C. Slattery, *Momentum, Energy and Mass Transfer in Continua*. Kreiger Press, New York (1978).
7. D. L. Koch and J. F. Brady, The effective diffusivity of fibrous media, *A.I.Ch.E. Jl* **32,** 575–591 (1986).
8. G. S. Beavers and E. M. Sparrow, Non-Darcy flow through fibrous porous media, *J. Appl. Mech.* **36,** 711–714 (1969).
9. C. L. Tien and K. Vafai, Statistical bounds for the effective thermal conductivity of microsphere and fibrous insulation, *Prog. Astronaut. Aeronaut.* **65,** 135–148 (1979).
10. F. M. White, *Viscous Fluid Flow*. McGraw-Hill, New York (1974).
11. R. E. Lundberg, P. A. McCuen and W. C. Reynolds, Heat transfer in annular passages. Hydrodynamically developed laminar flow with arbitrarily prescribed wall temperature or heat fluxes, *Int. J. Heat Mass Transfer* **6,** 495–529 (1963).

EFFETS DE DISPERSION THERMIQUE SUR LA CONVECTION FORCEE DANS LES MILIEUX FIBREUX

Résumé—L'étude expérimentale concerne l'écoulement non darcien et le transfert de chaleur dans les milieux fibreux à haute porosité. On considère la convection forcée à travers les matériaux de différentes perméabilités, porosités et conductivités thermiques. Les résultats montrent que les milieux poreux accroissent le transfert de chaleur à partir d'une surface, en comparaison avec les résultats calculés pour l'écoulement piston ou laminaire dans un canal. Cet accroissement résulte de la diffusion, un phénomène non darcien qui décrit le mélange intra-pore qui apparait quand le fluide se déplace entre les particules solides. Le transport dispersif augmente avec le flux d'écoulement et la perméabilité, et aux grands nombres de Reynolds il dépasse l'effet de la conduction dans le solide fibreux. Pour calculer la dispersion, ce travail développe un modèle simple basé sur les conditions d'écoulement et les types de milieux poreux. Les résultats de l'expérience et du modèle illustrent les effets de la dispersion et la pertinence de l'équation d'énergie homogène fluide–solide pour modéliser le transfert.

AUSWIRKUNGEN DER THERMISCHEN DISPERSION AUF DIE ERZWUNGENE KONVEKTION IN FASERFÖRMIGEN MEDIEN

Zusammenfassung—Die Nicht-Darcy-Strömung und die Wärmeübertragung in hochporösen faserförmigen Stoffen wird experimentell untersucht. Erzwungene Konvektion durch Materialien verschiedener Permeabilität, Porosität und Wärmeleitfähigkeit werden betrachtet. Die Ergebnisse zeigen die Verbesserung des Wärmeübergangs an einer Oberfläche in dem porösen Medium im Vergleich zu den berechneten Ergebnissen für eine Kolbenströmung oder laminare Kanalströmung. Diese Verbesserung rührt von der Dispersion her, einem Nicht-Darcy-Vorgang, welcher die intraporöse Mischung beschreibt, die sich vollzieht, wenn das Fluid an den festen Partikeln vorbeiströmt. Der dispersive Transport nimmt mit der Durchflußleistung und der Permeabilität zu und übersteigt bei hohen Reynolds-Zahlen den Transport durch Wärmeleitung im festen Teil des faserförmigen Mediums. Um die Dispersion vorauszubestimmen, wurde im Rahmen dieser Arbeit ein einfaches Modell entwickelt, das auf den Strömungsverhältnissen und der Form des porösen Mediums basiert. Die Ergebnisse aus Experiment und Modellrechnung zeigen den Einfluß der Dispersion und rechtfertigen das Modell, welches auf einer homogenen Fluid-Festkörper-Energiegleichung beruht.

ВЛИЯНИЕ РАСТЕКАНИЯ ТЕПЛА НА ВЫНУЖДЕННУЮ КОНВЕКДИЮ В ВОЛОКНИСТЫХ СРЕДАХ

Аннотация—Экспериментально изучаются течение, не подчиняющееся закону Дарси, и теплоперенос в высокопористых волокнистых средах. Рассматривается вынужденная конвекция через материалы различной проницаемости, пористости и теплопроводности. Показано, что в пористой среде перенос тепла от поверхности выше, чем для стержневого или ламинарного течения в канале. Это усиление является результатом растекания и отклонения от закона Дарси. Теплоперенос увеличивается с ростом скорости течения и проницаемости и при больших числах Рейнольдса превосходит кондуктивный перенос твердого остова волокнистой среды. Для расчета растекания тепла разработана простая модель, базирующаяся на режимах течения и типах пористых сред. Экспериментальные результаты и данные, полученные с помощью предложенной модели, демонстрируют влияние теплопереноса и адекватность уравнения энергии для системы однородная жицкость–твердое тело при моделировании переноса.